Thermoelectric Properties of Pb and Sr Doped $Ca_3Co_4O_9$

Thermoelectric Properties of Pb and Sr Doped Ca$_3$Co$_4$O$_9$

Hiroshi Nakatsugawa[1], Hyeon Mook Jeong[1], Natsuko Gomi[1] and Hiroshi Fukutomi
[1]Graduate school of Engineering, Yokohama National University
79-5 Tokiwadai, Hodogaya-ku
Yokohama 240-8501, Japan

Rak Hee Kim[2]
[2]School of Advanced material Engineering, Changwon National University
9 Sarim-dong, Changwon
Gyeongnam 641-773, Korea

ABSTRACT

We have prepared polycrystalline specimens of [(Ca$_{1-x}$Pb$_x$)$_2$CoO$_3$]$_{0.62}$CoO$_2$ and [(Ca$_{1-y}$Sr$_y$)$_2$CoO$_3$]$_{0.62}$CoO$_2$ using the conventional solid-state reaction method, and investigated the Pb substitution effect on the thermoelectric and magnetic properties. With the Pb substitution, both the electrical resistivity and Seebeck coefficient do not change drastically. This is attributed to the carrier concentration of samples. Seebeck and Hall coefficient measurements reveal that the major charge carriers in the samples are holes, however, the carrier concentration does not change with increasing x. The neutron powder diffraction technique and the magnetic susceptibility measurements also reveal that Pb ions take divalent state in the rock salt type Ca$_2$CoO$_3$ block layer. The average valence state of Co ions in the CdI$_2$ type CoO$_2$ sheet was 3.1+ and that of Co ions in the block layer was 3.6+. The resulting dimensionless figure of merit for the $x = 0.02$ sample at room temperature becomes 0.024, which is approximately equal to the corresponding values of a polycrystalline sample of NaCo$_2$O$_4$.

INTRODUCTION

Since the discovery of large thermoelectric power in the layered compounds NaCo$_2$O$_4$ and Ca$_3$Co$_4$O$_9$,[1-4] misfit-layered cobalt oxides particularly have attracted much interest as candidates for thermoelectric (TE) materials. Figure 1 shows the initial structure model projected in perspective from b-axis (left) and from a-axis (right). As shown in Fig.1, the Crystal structure of Ca$_3$Co$_4$O$_9$ consists of an alternate stack of a distorted three-layered rock salt (RS)-type Ca$_2$CoO$_3$ block layer (BL) and a CdI$_2$-type CoO$_2$ conducting sheet parallel to the c-axis.[3, 5, 6] The CdI$_2$-type [CoO$_2$] subsystem and the RS-type [Ca$_2$CoO$_3$] BL subsystem have common a- and c-axes and beta angles. Owing to the size difference between the RS-type BL and the CoO$_2$ sheet, however, the compound has an incommensurate periodicity parallel to the b-axis. The resulting structural formula becomes [Ca$_2$CoO$_3$]$_p$CoO$_2$, where p equals $b_{CoO_2}/b_{Ca_2CoO_3}$ 0.62 is an oxygen nonstoichiometry. The chemical formula can be approximately represented as Ca$_{1.24}$Co$_{1.62}$O$_{3.86}$. Throughout this paper, we will use the structural formula of the compound instead of the chemical formula. Such an anisotropic structure of the compound is believed to be favorable in realizing large absolute value of Seebeck coefficient, S, and low thermal conductivity, κ, necessary for good TE compounds. Furthermore, the RS-type BL can be regarded as a charge reservoir, which introduces hole carriers into the CoO$_2$ sheet. In addition, a CoO$_2$ triangular

lattice in the CoO$_2$ sheet should play an important role for realizing low electrical resistivity, ρ, namely, large TE power factor, S^2/ρ.
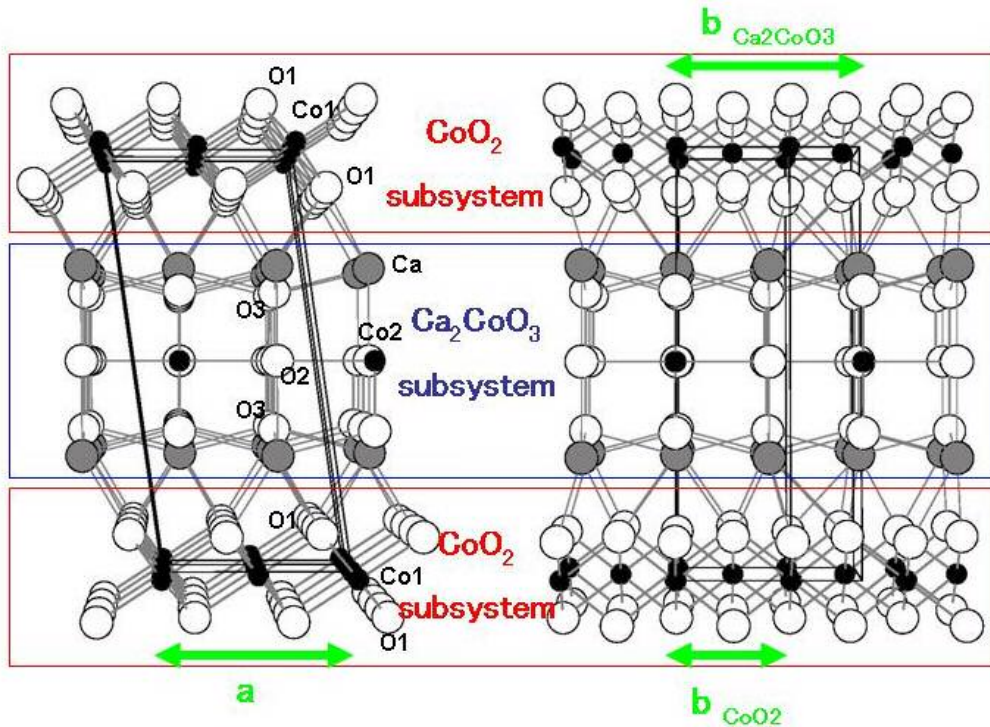
Fig. 1 Initial structure model of [Ca$_2$CoO$_3$]$_p$CoO$_2$.

As is well known, the *3d* orbital of an octahedrally coordinated Co ion splits into doubly degenerated upper e_g and triply degenerated lower t_{2g} levels. The t_{2g} levels further split into another doubly degenerated e_g' levels and a non-degenerated a_{1g} level due to the rhombohedral distortion of the octahedron. Since ^{59}Co NMR studies of metallic NaCo$_2$O$_4$ confirmed that both Co^{3+} and Co^{4+} ions are in the low-spin (LS) states,[7] the electronic configuration of each ion is Co^{3+}:$\left(e_g'\right)^4\left(a_{1g}\right)^2$ and Co^{4+}:$\left(e_g'\right)^4\left(a_{1g}\right)^1$, respectively. According to the band calculation of NaCo$_2$O$_4$,[8] the density of states (DOS) near the Fermi level (E$_F$) consists of the narrow (localized) a_{1g} band and the broad (itinerant) e_g' band. The height of E$_F$ depends on the nominal valence state of the Co ions. For the case of Co^{3+}, E$_F$ is located at the upper edge of the a_{1g} band, and therefore, high ρ is expected. With increasing hole carriers, the nominal valence state of the Co ions gradually close in Co^{4+} and E$_F$ crosses the bands , where a_{1g} and e_g' are hybridized. Thus, low ρ is then expected for such a mixed valent compound.

The polycrystalline Ca$_3$Co$_4$O$_9$ sample typically exhibits S　130 $\mu V/K$, ρ　1.5×10^{-4} Ωm and κ　$1.0\ W/mK$ at room temperature.[4] For practical use, an appreciable decrease in ρ must be achieved because ρ　1.5×10^{-4} Ωm at room temperature is about one order of magnitude higher than that of Bi$_2$Te$_3$-based TE materials. Much effort has been devoted to decrease ρ while maintaining a large S and low κ, through partial substitutions for Ca

atoms in the RS-type BL. The optimization of the valence state of Co ions in the RS-type BL is a key issue to maximize the TE properties because ρ and S are highly dependent on the nominal valence state of Co ions in the CoO_2 sheet. In fact, Li *et al.*[9] and Funahashi *et al.*[10] reported a marked increase in TE performance by partial substitution of Bi for Ca. However, no studies have ever tried to report the effect of Pb-substitution for Ca. Thus, we have employed a high-resolution neutron powder diffraction technique to investigate the modulated crystal structure of the Pb and Sr doped $[Ca_2CoO_3]_{0.62}CoO_2$ polycrystalline samples. This paper is intended as an investigation of the neutron powder diffraction technique and also measurements of electrical resistivity, Seebeck coefficient, Hall coefficient, thermal conductivity and magnetic susceptibility to clarify both the TE properties and the valence state of Co ions.

EXPERIMENT

The polycrystalline specimens of $[(Ca_{1-x}Pb_x)_2CoO_3]_{0.62}CoO_2$ and $[(Ca_{1-y}Sr_y)_2CoO_3]_{0.62}CoO_2$ were prepared by the conventional solid-state reaction method starting from powder mixture of $CaCO_3$ (99.9 %), $SrCO_3$ (99.9%), PbO (99.9 %) and Co_3O_4 (99.9 %) with a stoichiometric cation ratio. After calcination in air at 920 ℃ for 12 h, the calcined powders were pressed into pellets and sintered in pure flowing oxygen gas at 920 ℃ for 24 h. The obtained well-crystallized single-phase samples were annealed in pure flowing oxygen gas at 700 ℃ for 12 h and then quenched into distilled water to control oxygen nonstoichiometry.[11] Through the synthesis, the nominal *b*-axis ratio $b_{CoO_2}/b_{Ca_2CoO_3}$ was fixed at about 0.62 in all samples.

Neutron powder diffraction (ND) data were collected at room temperature using the Kinken powder diffractometer for high efficiency and high resolution measurements (HERMES) of Institute for Materials Research (IMR), Tohoku University, installed at the JRR-3M reactor in Japan Atomic Energy Research Institute (JAERI), Tokai.[12] Neutrons with a wavelength of 0.18265 nm were obtained by the 331 reflection of the Ge monochromator. The ND data were collected on thoroughly ground powders by a multiscanning mode in the 2θ range from $3.0°$ to $153.9°$ with a step width of $0.1°$ and were analyzed using a Rietveld refinement program, PREMOS 91,[13] adopting a superspace group of *C2/m(1p0)s0*, where the CdI_2 - type $[CoO_2]$ subsystem has *C2/m* symmetry while the RS – type BL $[Ca_2CoO_3]$ subsystem has *C2₁/m* symmetry. The crystal structures and interatomic distance plots were obtained with the use of PRJMS and MODPLT routines, respectively; both were implemented in the PREMOS 91 package.

Measurements of electrical resistivity, Seebeck coefficient and Hall coefficient were carried out in temperature range from 80 K to 385 K. The electrical resistivity, ρ, was measured by the van der Pauw technique with a current of 10 mA in He atmosphere. The Seebeck coefficient, S, measurement was carried out on a sample placed between two blocks of oxygen-free high conductivity (OFHC) silver. The thermocouples were welded to the reverse sides of the OFHC silver to measure temperature difference ΔT $3\ K$ and thermoelectric power, ΔV. The slope ($d\Delta V/d\Delta T$) obtained by the least-squares method yields the Seebeck coefficient, S, at each measurement temperature. The Hall coefficient, R_H, measurement was performed on flat square pieces of materials with a current of 100 mA in a magnetic field of 8500 Oe by the van der Pauw technique. The Hall carrier concentration n was determined from R_H using $n = 1/eR_H$, where e is the electron charge, assuming a scattering factor equal to 1 and a single

carrier model. Furthermore, the Hall mobility, μ, was determined from ρ and R_H using

$$\mu = R_H/\rho.$$

Thermal conductivity was measured at room temperature and magnetic susceptibility measurements were carried out in the temperature range from 2 K to 350 K. The thermal conductivity, κ, was calculated from $\kappa = A \cdot C \cdot D$, where A is the thermal diffusivity, C is the specific heat and D is the measured sample density. The thermal diffusivity was measured using the laser flash method (ULVAC, TC-3000) at room temperature. The magnetic susceptibility, χ, was measured using a superconducting quantum interference device (SQUID) magnetometer (Quantum Design, MPMS) under the zero-field cooling (ZFC) and field cooling (FC) conditions in a magnetic field of 10 Oe.

RESULTS AND DISCUSSION

Figure 2 shows the temperature dependence of the electrical resistivity of the specimens with $[(Ca_{1-x}Pb_x)_2CoO_3]_{0.62}CoO_2$ and $[(Ca_{1-y}Sr_y)_2CoO_3]_{0.62}CoO_2$ measured at the temperature range from 80 K to 385 K. In particular, the sample with $x = 0.02$ shows lowest electric resistivity, 1.67×10^{-4} Ωm at room temperature. All the samples show metallic behavior down to around 90 – 100 K. With further decrease in the temperature, the samples turn to be semiconducting behavior due to a carrier localization of a ferrimagnetic transition at around 20 K and the possible occurrence of the spin-density-wave (SDW) at around 100 K. Sugiyama et al.[14] have suggested that Co^{4+} ions in the RS – type BL play an important role in including the SDW transition. Furthermore, it is reported that the ferrimagnetic transition is originated from the modulated magnetic sublattices of Co^{4+} ions in the BL subsystem.[14]
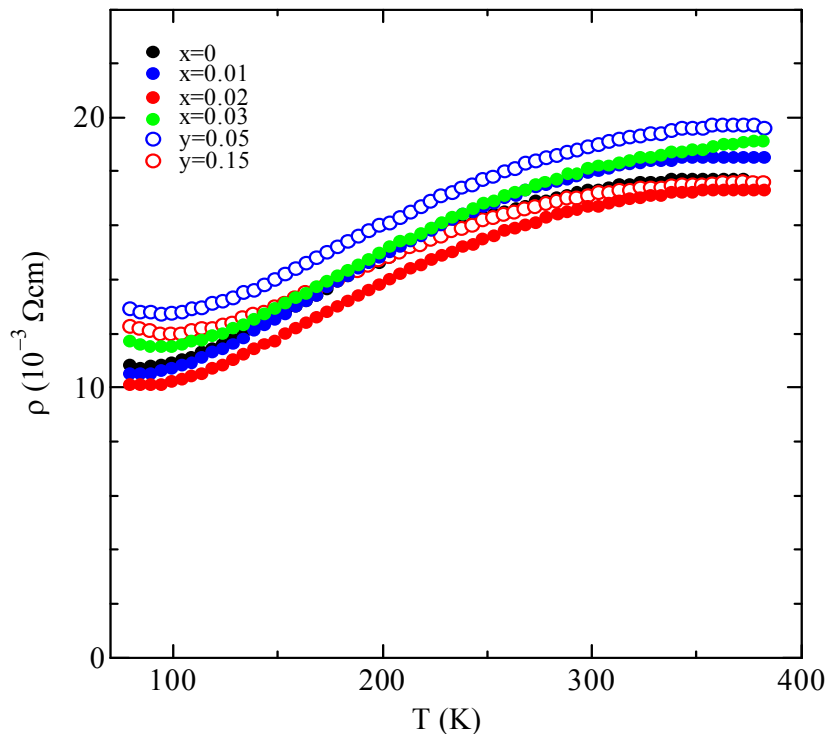
Fig. 2 Temperature dependence of the electrical resistivity ρ

The temperature dependence of the absolute value of Seebeck coefficient is shown in Fig.3. It can be seen clearly that at the temperatures above 100 K the Seebeck coefficient of $[(Ca_{1-x}Pb_x)_2CoO_3]_{0.62}CoO_2$ and $[(Ca_{1-y}Sr_y)_2CoO_3]_{0.62}CoO_2$ compounds shows weak temperature dependence. We have confirmed that all the samples have been found to show similar S. The effect of the Pb^{2+} substitution on the S values could be interpreted by the framework of the model which was proposed to explain the large Seebeck coefficient of the $NaCo_2O_4$. In that model, the Seebeck coefficient of high temperature limit can be estimated by using the modified Heikes formula: [15]

$$S(T \to \infty) = -\frac{k_B}{e} \ln\left[\frac{g_3}{g_4}\frac{c}{1-c}\right]$$

, where g_3, g_4 are the number of the degenerated configurations of the Co^{3+} and Co^{4+} states in the CoO_2 sheet while $c = Co^{4+}/Co$ is the fraction of Co^{4+} holes on the Co sites in the $[CoO_2]$ subsystem. Since the electronic configuration of Co^{3+} and Co^{4+} ion is the low spin state, the number of the degenerated configurations of the Co^{3+} and Co^{4+} states in the CoO_2 sheet is $g_3 = 1$ and $g_4 = 6$, respectively. Thus according to the above formula, the $S(T \to \infty)$ values would be steady with no change in c value. In the present study, the substitution of divalent Pb^{2+} for divalent Ca^{2+} would keep the hole concentrations. Therefore, $[(Ca_{1-x}Pb_x)_2CoO_3]_{0.62}CoO_2$ and $[(Ca_{1-y}Sr_y)_2CoO_3]_{0.62}CoO_2$ compounds shows similar S as shown in Fig.3.
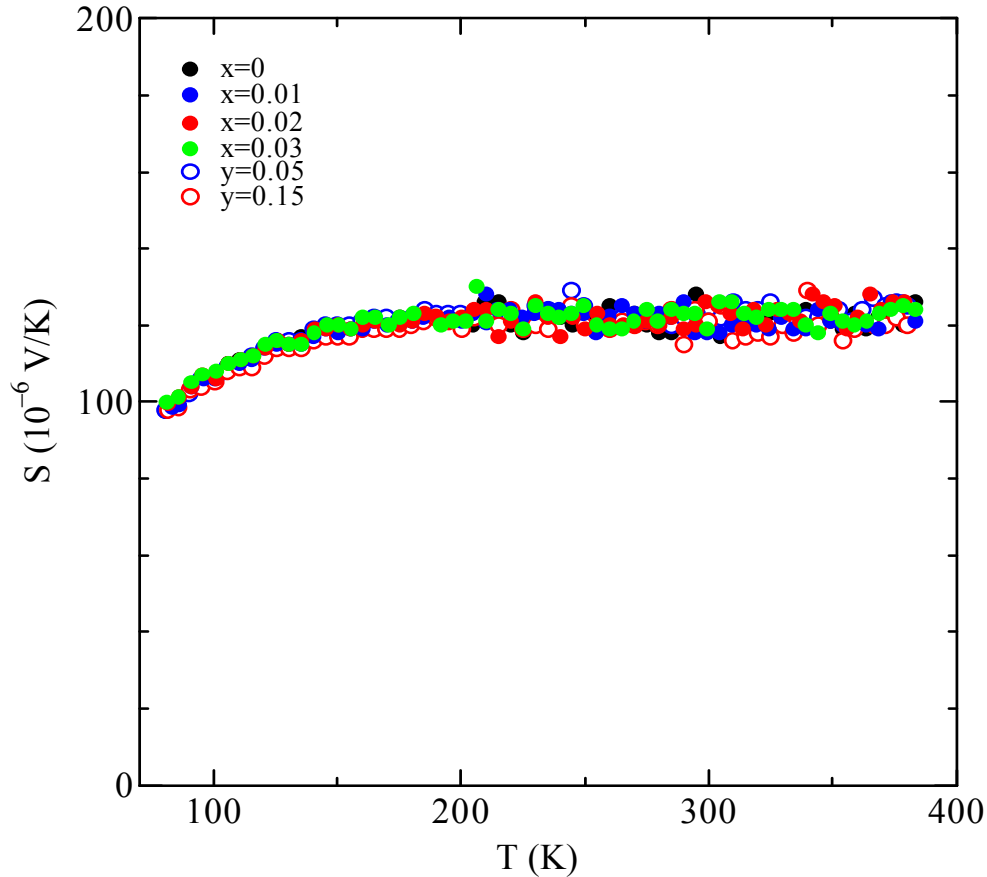
Fig. 3 Temperature dependence of Seebeck coefficient S

The TE power factor, S^2/ρ, of $[(Ca_{1-x}Pb_x)_2CoO_3]_{0.62}CoO_2$ and $[(Ca_{1-y}Sr_y)_2CoO_3]_{0.62}CoO_2$ as a function of temperature is represented in Fig.4. In particular, the sample with $x = 0.02$ exhibits largest TE power factor, $9.5\times10^{-5}\ W/mK^2$ at room temperature and shows a broad maximum at around $100 - 150$ K. With further decrease in temperature, the S^2/ρ value decreases gradually. Since the Seebeck coefficient $S(T)$ behavior does not change very much, as we have mentioned before, the TE power factor is primarily dependent on the value of electrical resistivity $\rho(T)$.
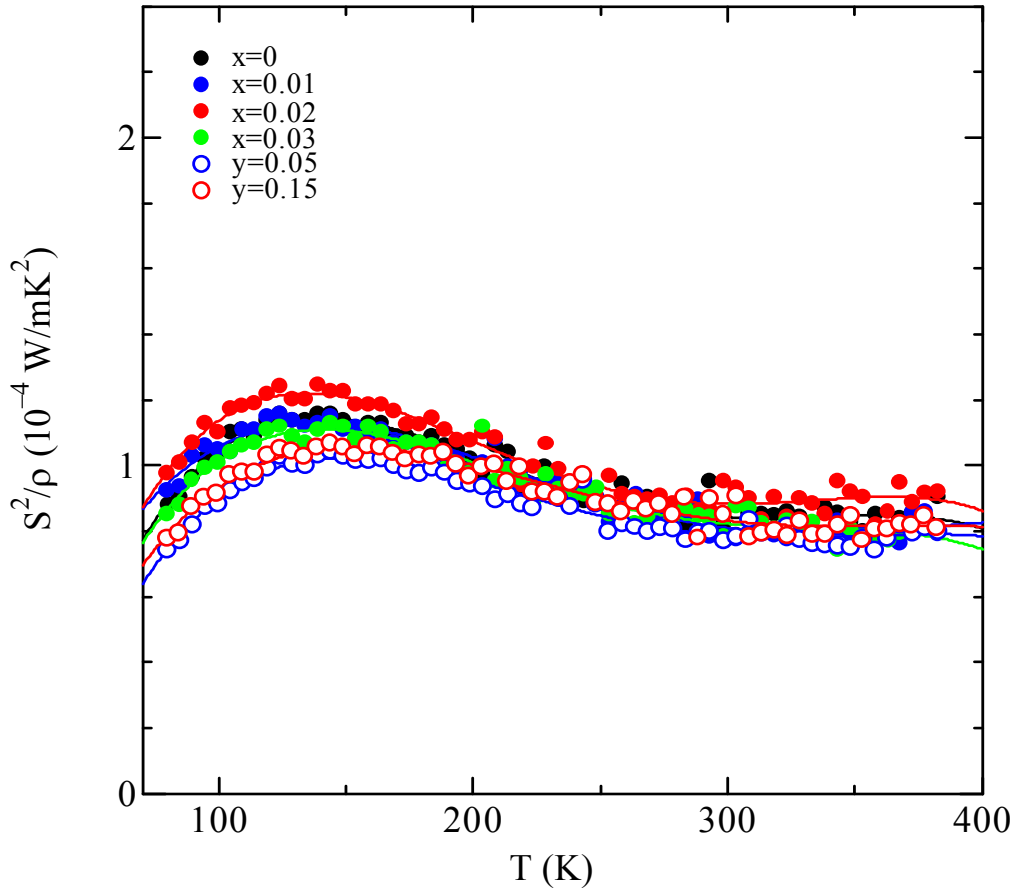
Fig. 4 Temperature dependence of the power factor S^2/ρ

Figure 5 shows the temperature dependence of the Hall coefficient $R_H(T)$ of the samples with $[(Ca_{1-x}Pb_x)_2CoO_3]_{0.62}CoO_2$ and $[(Ca_{1-y}Sr_y)_2CoO_3]_{0.62}CoO_2$ measured at the temperature range from 80 K to 385 K. All the samples show a positive value of R_H and similar values. Hall coefficient measurements reveal that the major charge carriers in all the samples are holes. Moreover, the signs of Hall coefficient were consistent with those of Seebeck coefficient. Hall carrier concentration $n = 1/eR_H$ and Hall mobility $\mu = R_H/\rho$ at room temperature are also shown in insets.
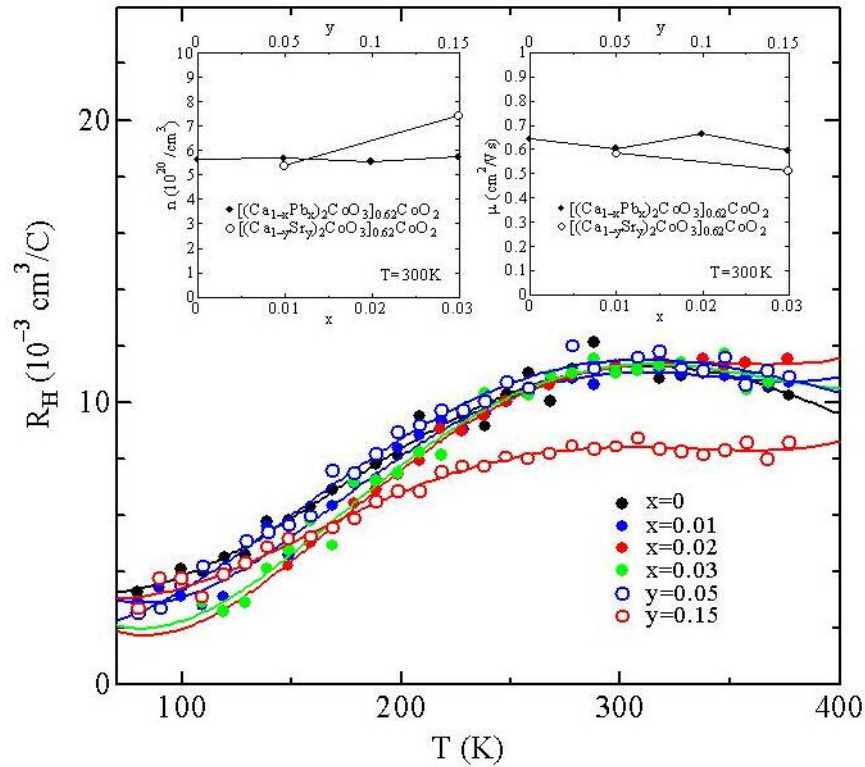
Fig. 5 Temperature dependence of the Hall coefficient R_H

We assume that the Pb atoms can only substitute for Ca. site. Figure 6 shows the observed, calculated and difference intensities of the HERMES data for $x = 0.02$ sample. The final R_{wp} factor was 8.0 % and the lattice parameters were refined to $a = 0.48384(3)$ nm, $b_{CoO_2} = 0.28248(1)$ nm, $c = 1.08865(6)$ nm and $\beta = 98.19(1)^\circ$ for [CoO$_2$] subsystem and $b_{RS} = 0.45786(7)$ nm for RS-type subsystem. The resulting $p = b_{CoO_2}/b_{Ca_2CoO_3} = 0.6169(5)$ corresponds to the stoichiometry of the $x = 0.02$ sample, i.e., [(Ca$_{0.98}$Pb$_{0.02}$)$_2$CoO$_3$]$_{0.6169}$CoO$_2$.
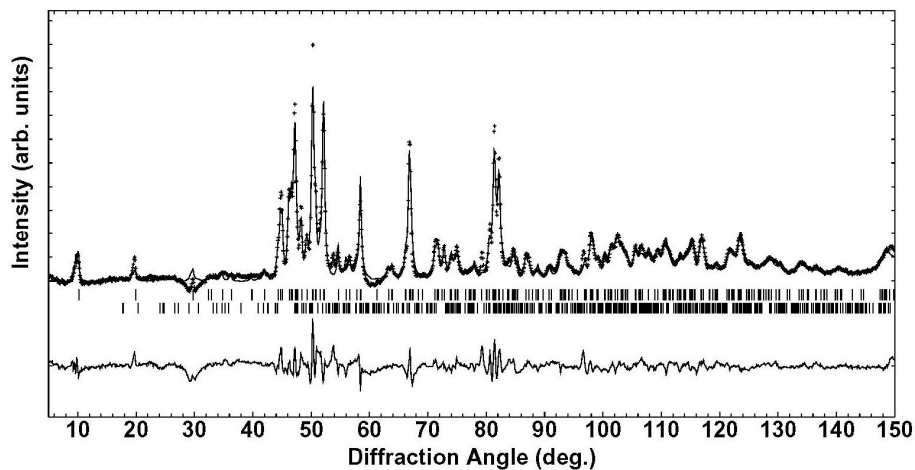
Fig. 6 Observed, calculated and difference intensities of powder neutron diffraction data

The variation of the atomic positional modulation can be further understood by the plot against t', a complementary coordinate in the (3+1)-dimensional superspace.[13] In the present samples, t' is defined as $-px_2 + x_4 \quad -0.62x_2 + x_4$. Figure 7 shows Co1 − O (upper panels) distances in the [CoO$_2$] subsystem and Co2 − O (lower panels) distances in the RS-type subsystem of (a) $x = 0$ (left) and (b) $x = 0.02$ (right) plotted against t'. Co2 site at $z = 1/2$ has six oxygen neighbors, with four equatorial O2 and two apical O3 atoms. Among these bonds, two apical Co2 − O3 bonds are fairly shorter than the other four equatorial Co2 − O2 bonds, ranging from 0.17 to 0.195 nm for $x = 0$ and from 0.165 to 0.19 nm for $x = 0.02$. The mean distance of Co2 − O3 bonds for $x = 0$ does not change very much as that of Co2 − O3 bonds for $x = 0.02$, i.e., both distances are 0.18 nm. This fact indicates that the Co ions in the RS-type subsystem are not replaced by tetravalent lead ions in the x range from 0 to 0.02. On the other hand, the four equatorial Co2 − O2 bonds for $x = 0$ (lower left panel) show small modulation amplitudes from 0.205 and 0.275 nm, relative to the $x = 0.02$ (lower right panel) of 0.18 and 0.3 nm. However, the mean distances of the Co2 − O2 bonds of the two phases are almost equal, i.e., 0.24 nm. In contrast to the Co2 − O bonds, the six Co1 − O1 bonds illustrated in the upper panels remain stable with increasing x, where the mean distance of the Co1 − O1 bonds is 0.19 nm.
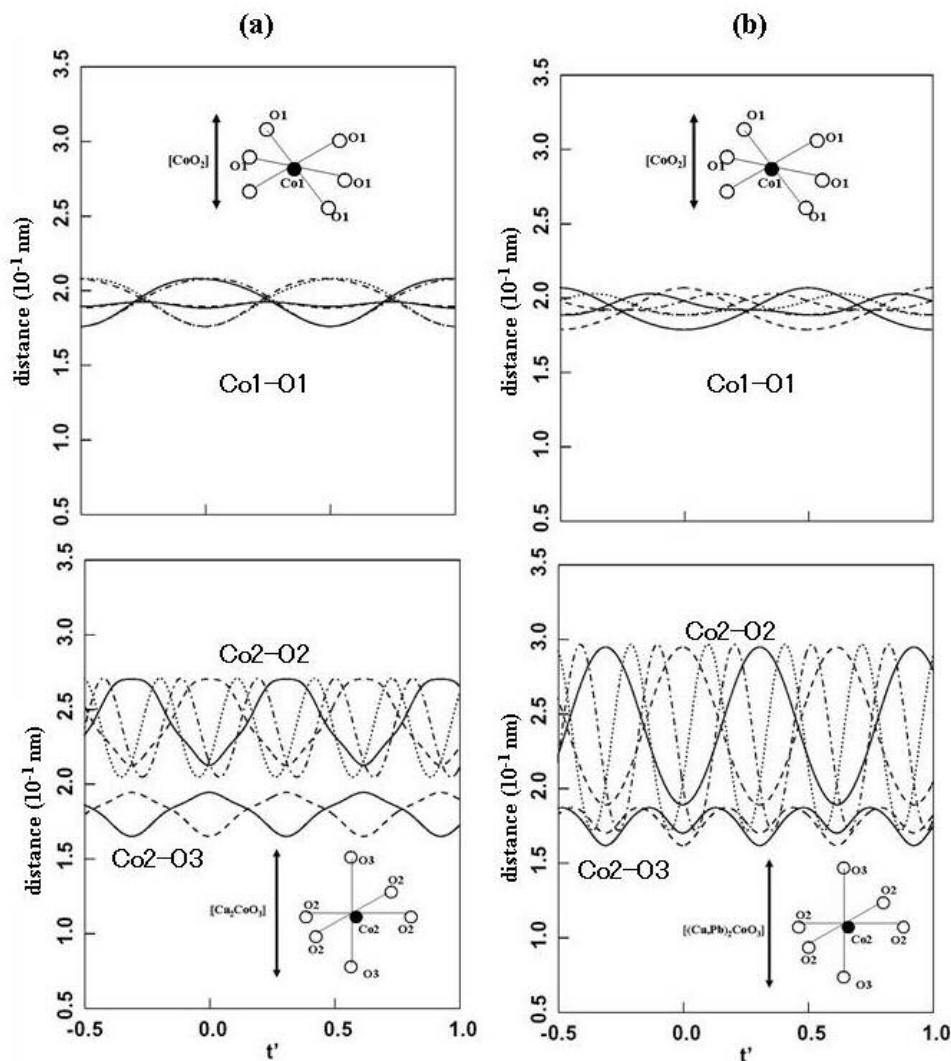
Fig. 7 Six Co1 − O1 distances (top left and right), four Co2 − O2 distances (bottom left and right) and two Co2 − O3 distances (bottom left and right) against a complementary coordinate, $t' = -px_2 + x_4 \quad -0.62x_2 + x_4$, in superspace for (a) x = 0 (left) and (b) x = 0.02 (right).

Relative to the Co – O distances, the (Ca, Pb) – O distances exhibit markedly change, due to the Pb substitution as demonstrated in Figs. 8(a) and 8(b), respectively. As illustrated in Fig.8, (Ca, Pb) site at $z = 0.72 \sim 0.73$ are coordinated to an apical O2 atom and four equatorial O3 atoms in the RS-type subsystem (see lower panels) and three O1 atoms in the $[CoO_2]$ subsystem (see upper panels). The (Ca, Pb) – O1 distances vary as shown in the upper panels. In contrast, the (Ca, Pb) – O2 and (Ca, Pb) – O3 distances vary as illustrated in the lower panels. Since the O2 and O3 atoms belong to the same RS-type subsystem, the Ca – O2 and Ca – O3 distances in $x = 0$ are moderately altered between 0.23 and 0.26 nm (lower left panel) with a mean distance of 0.245 nm, which is comparable to the typical ionic Ca – O bond lengths. The (Ca, Pb) – O2 and (Ca, Pb) – O3 distances for $x = 0.02$ shift to a considerably longer range from 0.215 and 0.283 nm (lower right panel), then the mean distance of five bonds was found to change markedly (2.49 nm). This fact indicates that the divalent Ca^{2+} ions are partially replaced by the divalent Pb^{2+} ions with increasing x.
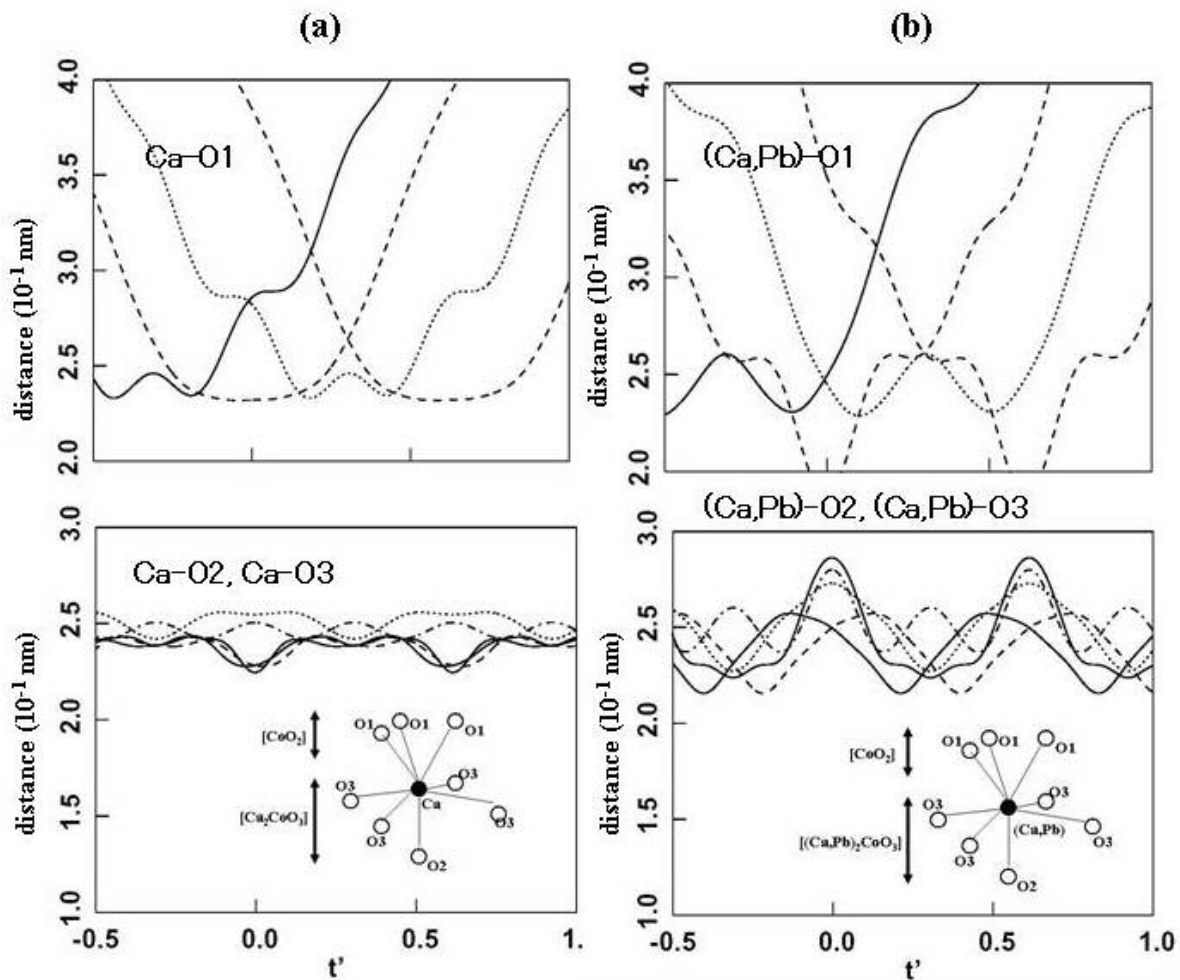
Fig. 8 Three Ca – O1 distances (top left), a Ca – O2 distance (bottom left) and four Ca – O3 distances (bottom left) against a complementary coordinate, $t' = -px_2 + x_4 \quad -0.62x_2 + x_4$, in superspace for (a) x = 0 (left). Three (Ca, Pb) – O1 distances (top right), a (Ca, Pb) – O2 distance (bottom right) and four (Ca, Pb) – O3 distances (bottom right) against a complementary coordinate t' in superspace for (b) x = 0.02 (right).

Let us evaluate the valence state of Co ions in $[(Ca_{1-x}Pb_x)_2CoO_3]_{0.62}CoO_2$ ($0 \leqq x \leqq 0.03$) assuming that the valence state of substituted lead ions are mainly divalent Pb^{2+}. Sugiyama *et al.*[14] have suggested that the polycrystalline $Ca_3Co_4O_9$ sample exhibits ferrimagnetic transition at T_C 19 K, due to an antiferromagnetic (AF) order of the Co1 in the $[CoO_2]$ subsystem and Co2 in the RS – type subsystem. Figure 9 represents the temperature dependence of the inverse-magnetic susceptibility, $(\chi - \chi_0)^{-1}$, of (a) $x = 0$, (b) $x = 0.01$, (c) $x = 0.02$ and (d) $x = 0.03$ measured ZFC condition in a magnetic field of 10 Oe.

(a)
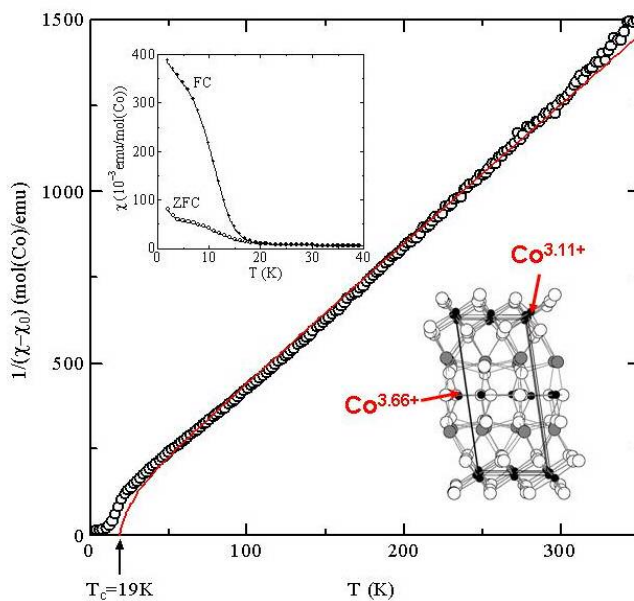
(b)
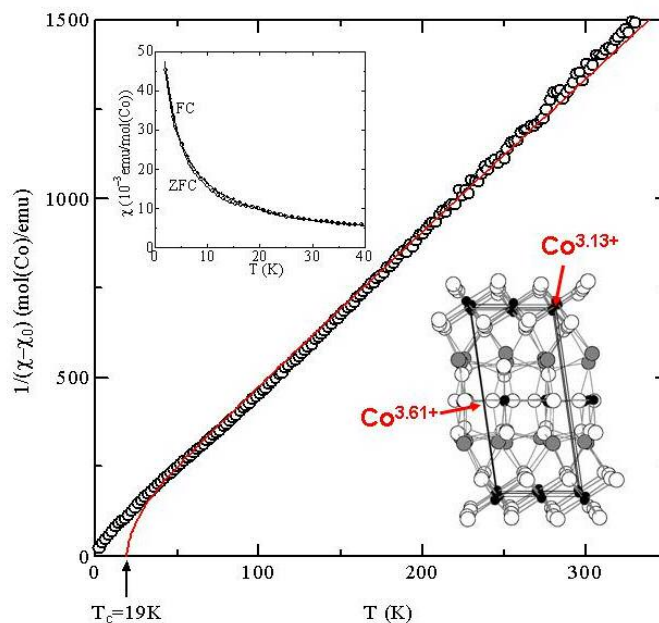
(c)
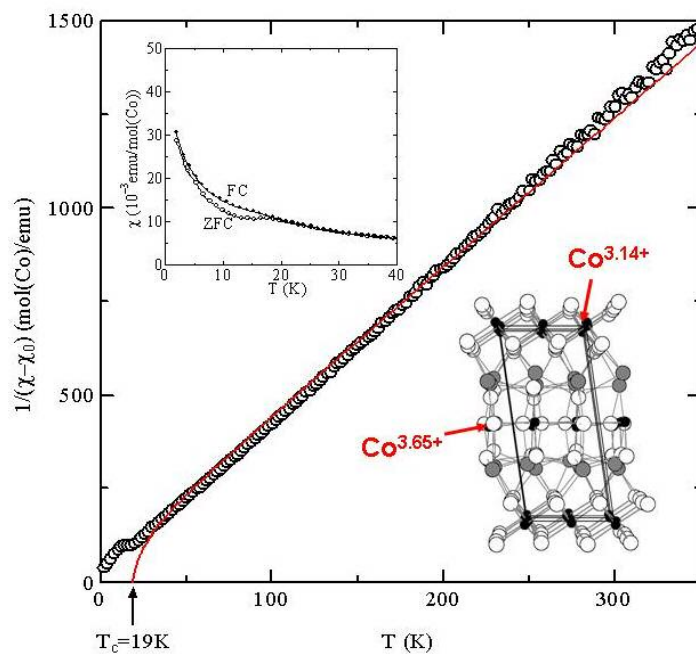
(d)
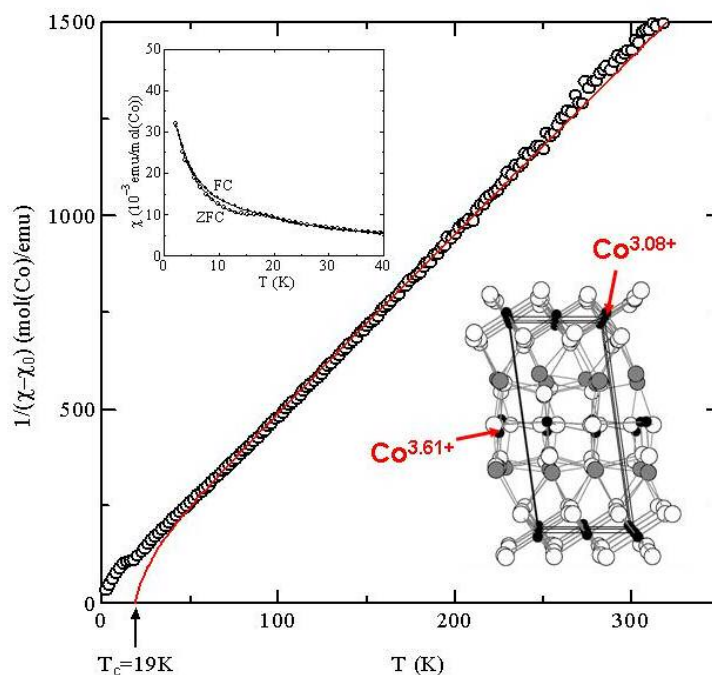
Fig. 9 Temperature dependence of inverse magnetic susceptibility $(\chi - \chi_0)^{-1}$, where red line shows appropriately fitting the $(\chi - \chi_0)^{-1}$ data, $\chi_0 \quad 7 \times 10^{-4} \, emu/mol(Co)$ is a temperature-independent term and $T_C = 19 \, K$ is a ferrimagnetic transition temperature. The insets show temperature dependence of magnetic susceptibility χ in a magnetic field of 10 Oe under ZFC (open circles) and FC (solid circles).

CONCLUSION

The polycrystalline specimens of have been prepared using the conventional solid-state reaction method, and the effect of Pb substitution on the TE properties have been studied. The sample with $x = 0.02$ shows rather low ρ and large S suggesting promising TE materials. Seebeck coefficient shows similar large S in all the samples because the substitution of Pb^{2+} for Ca^{2+} would keep the carrier (holes) concentration. In fact, the Co2 - O3 modulation reveal that Pb ions take mainly Pb^{2+} in the RS-type BL. The magnetic susceptibility measurements also show that Co1 and Co2 sites take the average valence state of $Co^{3.1+}$ and $Co^{3.6+}$, respectively. This suggests that Pb ions can hardly take Pb^{4+} in the RS-type BL of all samples.

ACKNOWLEDGMENTS

REFERENCES

[1] I. Terasaki, Y. Sasago and K. Uchinokura: Phys. Rev. B **56** (1997) R12685.

[2] S. Li, R. Funahashi, I. Matsubara, K. Ueda and H. Yamada: J. Mater. Chem. **9** (1999) 1659.

[3] A. C. Masset, C. Michel, A. Maignan, M. Hervieu, O. Toulemomde, F. Aruder, B. Raveau and J. Hejtmanek: Phys. Rev. B **62** (2000) 166.

[4] Y. Miyazaki, K. Kudo, M. Akoshima, Y. Ono, Y. Koike and T. Kajitani: Jpn. J. Appl. Phys. **39** (2000) L531.

[5] S. Lambert, H. Leligny and D. Grebille: J. Solid State Chem. **160** (2001) 322.

[6] Y. Miyazaki, M. Onoda, T. Oku, M. Kikuchi, Y. Ishii, Y. Ono, Y. Morii and T. Kajitani: J. Phys. Soc. Jpn. **71** (2002) 491.

[7] R. Ray, A. Ghoshray, K. Ghoshray and S. Nakamura: Phys. Rev. B **59** (1999) 9454.

[8] D. J. Singh: Phys. Rev. B **61** (2000) 13397.

[9] S. Li, R. Funahashi, I. Matsubara, K. Ueno, S. Sodeoka and H. Yamada: Chem. Mater. **12** (2000) 2424.

[10] R. Funahashi, I. Matsubara, H. Ikuta, T. Takeuchi, U. Mizutani and S. Sodeoka: Jpn. J. Appl. Phys. **39** (2000) L1127.

[11] J. Shimoyama, S. Horii, K. Otzschi, M. Sano and K. Kishio: Jpn. J. Appl. Phys. **42** (2003) L194.

[12] K. Ohoyama, T. Kanouchi, K. Nemoto, M. Ohashi, T. Kajitani and Y. Yamaguchi: Jpn. J. Appl. Phys. **37** (1998) 3319.

[13] A.Yamamoto: Acta Cryst. A **49** (1993) 831.

[14] J. Sugiyama, H. Itahara, T. Tani, J. H. Brewer and E. J. Ansaldo: Phys. Rev. B **66** (2002) 134413.

[15] W. Koshibae, K. Tsutsui and S. Maekawa: Phys. Rev. B **62** (2000) 6869.